

# Laplace domain BEM for anisotropic transient elastodynamics

**Ivan Markov** 

*National Research Lobachevsky State University of Nizhny Novgorod, Nizhny Novgorod, Russian Federation*

**Leonid Igumnov** 

*National Research Lobachevsky State University of Nizhny Novgorod, Nizhny Novgorod, Russian Federation*

**Aleksandr Belov** 

*National Research Lobachevsky State University of Nizhny Novgorod, Nizhny Novgorod, Russian Federation*

**Victor Eremeyev** 

*Department of Mechanics of Materials and Structures, Faculty of Civil and Environmental Engineering, Gdansk University of Technology, Gdansk, Poland; Department of Civil and Environmental Engineering and Architecture (DICAAR), University of Cagliari, Cagliari, Italy*

## Abstract

In this paper, we describe Laplace domain boundary element method (BEM) for transient dynamic problems of three-dimensional finite homogeneous anisotropic linearly elastic solids. The employed boundary integral equations for displacements are regularized using the static traction fundamental solution. Modified integral expressions for the dynamic parts of anisotropic fundamental solutions and their first derivatives are obtained. Boundary elements with mixed approximation of geometry and field variables with the standard nodal collocation procedure are used for spatial discretization. In order to obtain time-domain solutions, the classic Durbin's method is applied for numerical inversion of Laplace transform. Problem of alleviating Gibbs oscillations is addressed. Dynamic boundary element analysis of the model problem involving trigonal material is performed to test presented formulation. Obtained results are compared with finite element solutions.

## Keywords

Anisotropic elasticity, boundary element method, dynamic analysis, Laplace transform, Durbin's method

---

## Corresponding author:

Leonid Igumnov, National Research Lobachevsky State University of Nizhny Novgorod, 23 Gagarin Avenue, Building 6, Nizhny Novgorod 603950, Russian Federation.  
Email: [igumnov@mech.unn.ru](mailto:igumnov@mech.unn.ru)

## 1. Introduction

Although boundary element method (BEM) is a very useful and powerful numerical method applied to various fields of engineering analysis, its application within anisotropic elasticity is somewhat difficult due to unavailability of closed-form analytical fundamental solutions for the both statics and dynamics of anisotropic solids [1–10]. Static anisotropic elastic (and with coupled fields) fundamental solutions are extensively investigated and many different approaches for their calculation have been proposed over the last years [11,12]. Most commonly used practical application form of regular part of the three-dimensional frequency-domain dynamic anisotropic elastic fundamental solution is derived using Radon transform. It has very complex structure and is expressed as an integral over the surface of a half of a unit sphere [13,14].

Wave propagation phenomenon has been extensively studied in various applications. Especially, as the design of advanced materials is becoming a topical subject [15], investigation of such phenomena becomes more and more important to conceive new materials (“metamaterials”), for example, pantographic metamaterials, the macroscopic mechanical properties of which are mostly defined by the structure of the metamaterial at the micro and nano scale [16–19]. Verification of theoretical investigations of designed models and determination of constitutive parameters are frequently performed by numerical modeling [20–23]. The BEM and the Green’s function method can be very useful for numerical solution of boundary value problems involving such metamaterials [24,25].

In this paper, we present a conventional direct Laplace domain boundary element approach for analysis of the wave propagation in anisotropic linearly elastic finite solids. The static anisotropic elastic traction fundamental solution is used to regularize the boundary integral equations. Modified integral expressions for the dynamic parts of the fundamental solutions are employed. Standard nodal collocation procedure and mixed boundary elements are used for spatial discretization. Classic Durbin’s method [26] for numerical inversion of Laplace transform is utilized to obtain solutions in the time domain. Frequency-domain data windowing technique is applied to alleviate Gibbs oscillations. Boundary element results for the model numerical example involving trigonal material are compared with the solutions obtained with the finite element method (FEM).

## 2. Problem statement and BEM formulation

Let us consider a three-dimensional, homogeneous, anisotropic, and linearly elastic solid body occupying a bounded volume  $\Omega \in R^3$  with a surface  $\Gamma = \partial\Omega$ . Under the assumption of absent body forces and zero initial conditions, the equations of motion in the Laplace domain are given by

$$\bar{\sigma}_{ij,j}(\mathbf{x}, s) - \rho s^2 \bar{u}_i(\mathbf{x}, s) = 0, \mathbf{x} \in \Omega, i, j = 1, 2, 3, \quad (1)$$

where  $\bar{\sigma}_{ij}$ ,  $\rho$ ,  $s$ , and  $\bar{u}_i$  are the stress, mass density, the Laplace transform parameter, and displacement, respectively.

Constitutive law is written as Hooke’s law:

$$\bar{\sigma}_{ij}(\mathbf{x}, s) = C_{ijkl} \bar{\varepsilon}_{kl}(\mathbf{x}, s), k, l = 1, 2, 3, \quad (2)$$

where  $C_{ijkl}$  is a constant fourth-order elastic stiffness tensor and does not depend on spatial variable  $\mathbf{x}$ , that is, material is assumed to be homogeneous. The elasticity tensor satisfies the following symmetry relations:  $C_{ijkl} = C_{jikl} = C_{ijlk} = C_{klij}$ .

Considering small deformations, the strain–displacement relationship is given by

$$\bar{\varepsilon}_{ij}(\mathbf{x}, s) = \frac{1}{2} (\bar{u}_{i,j}(\mathbf{x}, s) + \bar{u}_{j,i}(\mathbf{x}, s)), \quad (3)$$

where  $\bar{\varepsilon}_{ij}$  is the symmetric linear strain tensor, and with subscript after comma we denote a spatial partial derivative.

Substituting equation (3) into equation (2) and then the result into equation (1), the dynamic equations take the following form:

$$C_{ijkl}\bar{u}_{k,lj}(\mathbf{x}, s) - \rho s^2 \bar{u}_i(\mathbf{x}, s) = 0, \mathbf{x} \in \Omega. \quad (4)$$

For a mixed boundary value problem, the boundary conditions are given by

$$\bar{u}_i(\mathbf{x}, s) = \bar{u}_i^*(\mathbf{x}, s), \mathbf{x} \in \Gamma_u, \quad (5)$$

$$\bar{t}_i(\mathbf{x}, s) = \bar{\sigma}_{ik}(\mathbf{x}, s)n_k(\mathbf{x}) = \bar{t}_i^*(\mathbf{x}, s), \mathbf{x} \in \Gamma_t, \quad (6)$$

where  $n_k$  is the outward normal to the boundary  $\Gamma$  at  $\mathbf{x}$ ,  $\Gamma_u$  and  $\Gamma_t$  are the corresponding parts of the boundary, and  $\bar{u}_i^*(\mathbf{x}, s)$  and  $\bar{t}_i^*(\mathbf{x}, s)$  are given displacements and tractions.

Equivalent to equation (4), boundary integral equations (BIEs) for displacements are regularized using the static anisotropic elastic traction fundamental solution  $h_{jk}^S(\mathbf{y}, \mathbf{x})$ . They are weakly singular and have the following form:

$$\int_{\Gamma} \left[ \bar{u}_k(\mathbf{y}, s) \bar{h}_{jk}(\mathbf{y}, \mathbf{x}, s) - \bar{u}_k(\mathbf{x}, s) h_{jk}^S(\mathbf{y}, \mathbf{x}) - \bar{t}_k(\mathbf{y}, s) \bar{g}_{jk}(\mathbf{y}, \mathbf{x}, s) \right] d\Gamma(\mathbf{y}) = 0, j, k = 1, 2, 3, \quad (7)$$

where  $\mathbf{x} \in \Gamma$ ,  $\bar{g}_{jk}$ , and  $\bar{h}_{jk}$  denote Laplace domain displacement and traction dynamic fundamental solutions, respectively.

For the spatial discretization of BIEs (equation (7)), we employ boundary elements with quadratic interpolation. The simplest possible mixed representation of the field variables on the boundary elements is adopted. Displacements and tractions are approximated using different shape functions: linear and constant, respectively. This approach to discretization allows one correct modeling of discontinuous tractions while at the same time maintaining continuity of displacements. After following standard nodal collocation procedure and taking into account the prescribed boundary conditions, for a given value of Laplace transform parameter  $s$  we obtain the complex-valued resolving system of linear algebraic equations:

$$\mathbf{A}(s)\mathbf{p}(s) = \mathbf{f}(s), \quad (8)$$

where  $\mathbf{A}(s) \in \mathbb{C}^{N_{\text{dof}} \times N_{\text{dof}}}$  is the dense and asymmetric influence matrix,  $\mathbf{p} \in \mathbb{C}^{N_{\text{dof}} \times 1}$  contains unknown field variables, and elements of  $\mathbf{f} \in \mathbb{C}^{N_{\text{dof}} \times 1}$  are linear combination of integrals of the kernels in equation (7) corresponding to the prescribed boundary data;  $N_{\text{dof}}$  is the total number of degrees of freedom.

### 3. Fundamental solutions

Displacement and traction fundamental solutions in Laplace domain represented as a sum of static and dynamic parts as follows:

$$\bar{g}_{ij}(\mathbf{y}, \mathbf{x}, s) = \bar{g}_{ij}(\mathbf{r}, s) = g_{ij}^S(\mathbf{r}) + \bar{g}_{ij}^R(\mathbf{r}, s), j, k = 1, 2, 3, \quad (9)$$

$$\bar{h}_{mi}(\mathbf{y}, \mathbf{x}, s) = \bar{h}_{mi}(\mathbf{r}, s) = C_{ijkl}\bar{g}_{mk,l}(\mathbf{r}, s)n_j(\mathbf{y}) = h_{mi}^S(\mathbf{r}) + \bar{h}_{mi}^R(\mathbf{r}, s), m = 1, 2, 3, \quad (10)$$

$$\mathbf{r} = \mathbf{y} - \mathbf{x}, r = |\mathbf{r}|, \quad (11)$$

where  $n_j$  is outward unit normal of the boundary  $\Gamma$  at  $\mathbf{y}$ .

Following Wang and Achenbach [13,14], we employ integral expressions for the static and dynamic parts of the displacement fundamental solution. The integration for the dynamic part and its derivative takes over a half of a unit sphere  $|\mathbf{n}| = 1$  which is expressed in terms of spherical coordinates  $0 \leq \psi \leq \pi/2$  and  $0 \leq \varphi \leq 2\pi$ :

$$g_{ij}^S(\mathbf{r}) = \frac{1}{8\pi^2 r} \int_0^{2\pi} \int_0^{\pi/2} \Gamma_{ij}^{-1} \left( \mathbf{n} \left( \varphi, \frac{\pi}{2} \right) \right) d\varphi, \quad (12)$$

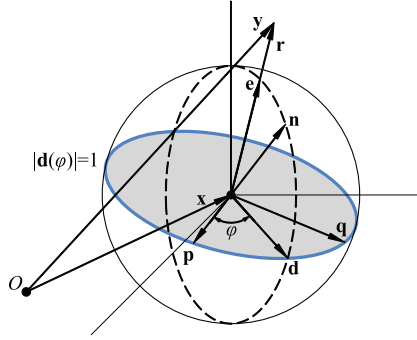


**Figure 1.** Illustration of vector  $\mathbf{n}$  and auxiliary variables.

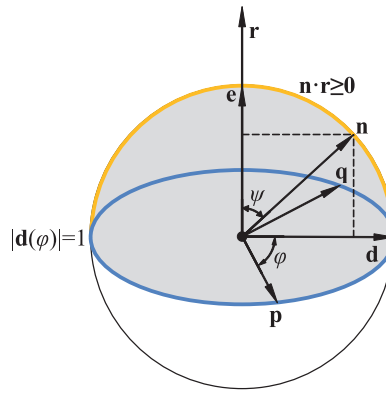


**Figure 2.** Close-up of variables required to define vector  $\mathbf{n}$ .

$$\bar{g}_{ij}^R(\mathbf{r}, s) = -\frac{s\sqrt{\rho}}{8\pi^2} \int_0^{2\pi} \int_0^{\pi/2} \sum_{m=1}^3 \frac{E_{im}E_{jm} \sin \psi}{\lambda_m^{3/2}} \exp\left(sr\sqrt{\rho}\left(-\frac{\cos \psi}{\sqrt{\lambda_m}}\right)\right) d\psi d\varphi, \quad (13)$$

$$\bar{g}_{ij,l}^R(\mathbf{r}, s) = \frac{s^2\rho}{8\pi^2} \int_0^{2\pi} \int_0^{\pi/2} \sum_{m=1}^3 \frac{n_l(\varphi, \psi)E_{im}E_{jm} \sin \psi}{\lambda_m^2} \exp\left(sr\sqrt{\rho}\left(-\frac{\cos \psi}{\sqrt{\lambda_m}}\right)\right) d\psi d\varphi, \quad (14)$$

$$c_m = \sqrt{\frac{\lambda_m}{\rho}}, k_m = \frac{s}{c_m}, \quad (15)$$

where  $\lambda_m$  and  $E_{jm}$  are the eigenvalues and the corresponding eigenvectors of the matrix  $\Gamma_{ij}(\mathbf{n}(\varphi, \psi)) = C_{kij}n_k n_l$ . Vector  $\mathbf{n}(\varphi, \psi)$  required in equations (12)–(15) is defined as follows (see also Figures 1 and 2):

$$\mathbf{n}(\varphi, \psi) = \mathbf{d}(\varphi) \sin \psi + \mathbf{e} \cos \psi = [n_1, n_2, n_3]^T, \quad (16)$$

$$\mathbf{d}(\varphi) \cdot \mathbf{r} = 0, \mathbf{e} = \frac{\mathbf{r}}{r}, \mathbf{e} = [e_1, e_2, e_3]^T, \quad (17)$$

$$\mathbf{p} = \frac{[e_2, -e_1, 0]^T}{\sqrt{1-e_3^2}}, \mathbf{q} = \mathbf{e} \times \mathbf{p} = \frac{[e_1 e_3, e_2 e_3, -(1-e_3^2)]^T}{\sqrt{1-e_3^2}}, \quad (18)$$



$$\mathbf{p} \cdot \mathbf{e} = 0, \mathbf{q} \cdot \mathbf{e} = 0, \mathbf{p} \cdot \mathbf{q} = 0, \mathbf{d}(\varphi) = \mathbf{p} \cos \varphi + \mathbf{q} \sin \varphi, 0 \leq \varphi \leq 2\pi, \quad (19)$$

$$\mathbf{d}(\varphi) = \frac{[e_2 \cos \varphi + e_1 e_3 \sin \varphi, -e_1 \cos \varphi + e_2 e_3 \sin \varphi, -(1 - e_3^2) \sin \varphi]^T}{\sqrt{1 - e_3^2}}. \quad (20)$$

#### 4. Numerical inversion of Laplace transform

The Laplace transform and its inversion are defined as follows:

$$F(s) = L\{f(t)\} = \int_0^{+\infty} e^{-st} f(t) dt, f(t) = 0 \text{ for } t < 0, s = \alpha + i\omega, \quad (21)$$

$$f(t) = L^{-1}\{F(s)\} = \frac{1}{2\pi i} \int_{\alpha - i\infty}^{\alpha + i\infty} e^{st} F(s) ds, \quad (22)$$

where  $\alpha$  is an arbitrary real number greater than the real parts of all the singularities of  $F(s)$ .

To obtain time-domain solutions, we employ classic well-known Durbin's method [26] to numerically invert the Laplace integral transform. Durbin's method is frequently used together with Laplace domain BEM and for solving wave propagation problems as in the most cases it can provide reliable results over all selected time range [27–33]. Durbin's method for real function  $f(t)$ , with  $f(t) = 0$  for  $t < 0$ , is based on the following equivalent representation of  $f(t)$ , which can be obtained after simple algebraic manipulations on the right-hand side of equation (22):

$$f(t) = \frac{e^{\alpha t}}{\pi} \int_0^{+\infty} [\operatorname{Re}(F(\alpha + i\omega)) \cos(\omega t) - \operatorname{Im}(F(\alpha + i\omega)) \sin(\omega t)] d\omega, t \geq 0. \quad (23)$$

Equation (23) corresponds to an integration along a straight line  $\operatorname{Re}(s) = \alpha$  parallel to the imaginary axis in the complex plane. The following approximation of the time-domain function  $f(t)$ , which is referred to as *Durbin's formula*, was obtained in Durbin [26] using a Fourier series expansion of  $e^{-\alpha t} f(t)$  on the time interval  $[0, 2T]$  and by cutting off an infinite series on  $N_{sum}$  terms:

$$f(t) \approx \frac{e^{\alpha t}}{T} \left[ -\frac{1}{2} \operatorname{Re}(F(\alpha)) + \sum_{k=0}^{N_{sum}} \left\{ \operatorname{Re} \left( F \left( \alpha + i \frac{k\pi}{T} \right) \right) \cos \left( \frac{k\pi}{T} t \right) - \operatorname{Im} \left( F \left( \alpha + i \frac{k\pi}{T} \right) \right) \sin \left( \frac{k\pi}{T} t \right) \right\} \right], \quad (24)$$

where  $0 \leq t \leq 2T$  is the considered time range for the inversion.

For BEM calculations, we restricted ourselves to certain values of  $\omega_{max}$  and  $t_{max}$ , which are the maximum value of imaginary part of complex Laplace transform parameter  $s$  and the maximum time that we are interested in, respectively. Taking it into consideration, the parameter  $T$  and the number of terms  $N_{sum}$  in the series can be determined by the following formulae:

$$2T > t_{max} \Rightarrow T > \frac{t_{max}}{2} \Rightarrow T = T^* t_{max}, T^* > 0.5, N_{sum} = \left\lceil \frac{\omega_{max} T^* t_{max}}{\pi} \right\rceil. \quad (25)$$

Relying on the results in Crump [34], we choose  $\alpha$  as

$$\alpha = \frac{\kappa \ln 10}{T} = \frac{\kappa \ln 10}{T^* t_{max}}, \kappa > 1.0. \quad (26)$$

So we identify  $\omega_{\max}$  and  $t_{\max}$  as the input parameters of the Durbin's method, and  $T^*$  and  $\kappa$  as the free parameters.

## 5. Numerical example

For the numerical example, we consider a model problem which is frequently used to test versatility and efficiency of boundary element approaches. An anisotropic elastic bar shown in Figure 3 with the length of 1 m and a square cross section of 0.2 m  $\times$  0.2 m is clamped at  $x_3 = 0$  m and subjected to a step load  $t_3 = PH(t)$ ,  $P = -1 \cdot 10^6$  Pa at the face  $x_3 = 1$  m.

Trigonal material (sapphire) of the mass density  $\rho = 3970$  kg/m<sup>3</sup> and of the following elastic moduli [7,35,36] is considered:

$$\mathbf{C} = \begin{bmatrix} 494 & 158 & 114 & -23 & 0 & 0 \\ & 494 & 114 & 23 & 0 & 0 \\ & & 496 & 0 & 0 & 0 \\ & & & 145 & 0 & 0 \\ \text{symm.} & & & & 145 & -23 \\ & & & & & 168 \end{bmatrix} \text{ GPa.}$$

Matrix  $\mathbf{C}$  is a positive definite as the corresponding complete necessary and sufficient conditions for it for a trigonal crystal [37] are satisfied, that is,  $c_{11} > |c_{12}|$ ,  $(c_{11} + c_{12})c_{33} > 2c_{13}^2$ , and  $(c_{11} - c_{12})c_{44} > 2c_{14}^2$ .

To obtain time-domain solutions in the boundary element analysis, we selected the following values of the input and free parameters in Durbin's method:

$$\omega_{\max} = 150,000 \frac{\text{rad}}{\text{s}}, \quad t_{\max} = 0.001 \text{ s}, \quad T^* = 1.65, \quad \kappa = 2.0.$$

By this way, the number of sampling frequencies became  $N_{\text{sum}} = 79$ .

First, we employ four different uniform meshes with 88 (denoted as mesh 1), 352 (mesh 2), 792 (mesh 3), and 1408 (mesh 4) quadrilateral boundary elements to test mesh convergence. Obtained results for displacements  $u_3(t)$  at point  $A$  (0.0, 0.0, 1.0) m located on the loaded face and at point  $B$  (0.0, 0.0, 0.5) m inside the bar are displayed in Figures 4 and 5, respectively. In Figures 6 and 7, the results for stress  $\sigma_{33}(t)$  at point  $B$  and point  $C$  (0.0, 0.0, 0.0) m are presented.

Obtained results are consistent throughout all the considered time range and the difference between the solutions with the refining of the mesh is quickly diminishing.

Next, we compare BEM solutions on mesh 4 with the results of the linear and full transient finite element analysis performed with Ansys software. System of equations was solved with a default solver. The uniform FEM model of the bar consists of 5000 twenty-node solid elements SOLID186, all comparison points located on the corresponding nodes of the FEM model. For a time-stepping scheme in a transient anisotropic elastodynamic analysis of a considered structure under impact load, where spurious

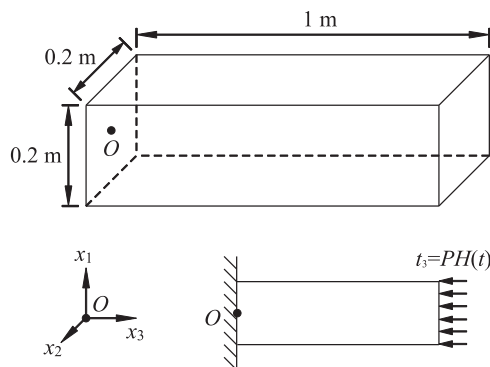
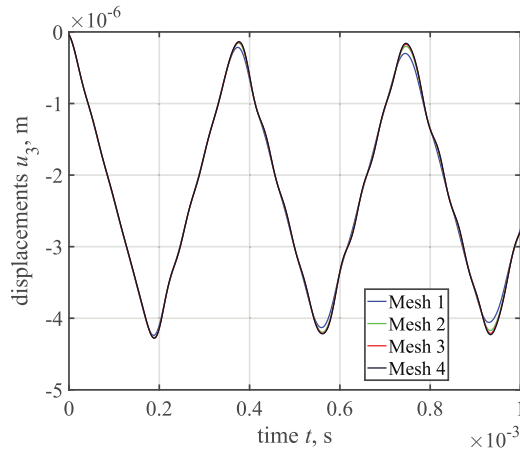
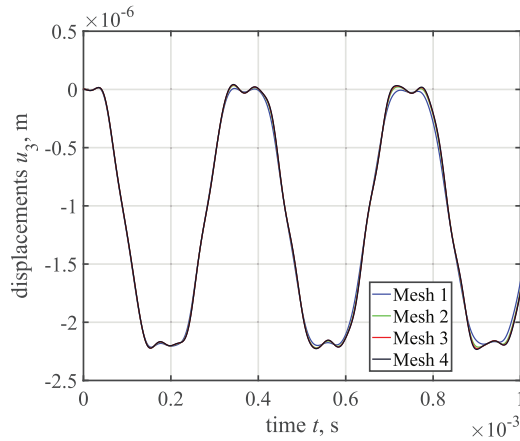


Figure 3. Anisotropic elastic bar under Heaviside load.





**Figure 4.** BEM solutions for displacements  $u_3(t)$  at point A.



**Figure 5.** BEM solutions for displacements  $u_3(t)$  at point B.

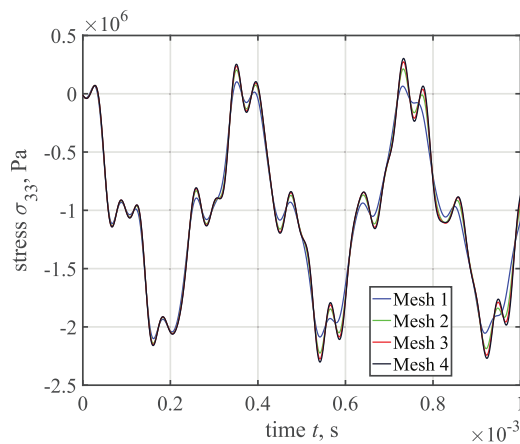


**Figure 6.** BEM solutions for stress  $\sigma_{33}(t)$  at point B.

oscillations (Gibbs phenomenon) occur near sharp gradients and discontinuities in structural response, we employ a damped Newmark's algorithm. Parameters of Newmark's method are as follows [38]:  $\alpha = 0.5$  and  $\delta = 0.7$ . When choosing  $\delta > 0.5$ , numerical dissipation is introduced ( $\delta = 0.5$  corresponds to an undamped version) [39] to damp out spurious high-frequency response. The maximum time is 0.001 s

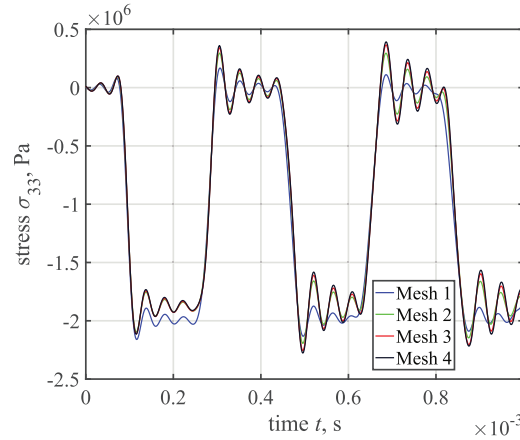


**Figure 7.** BEM solutions for stress  $\sigma_{33}(t)$  at point C.

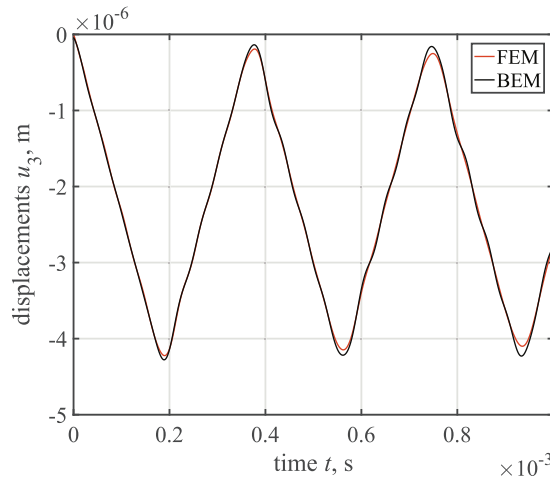


**Figure 8.** BEM and FEM solutions for displacements  $u_3(t)$  at point A.

and the total number of time steps is 930. Comparing the BEM and FEM results in Figures 8–11, we observe that solutions are in a good agreement. Slight decrease of amplitude of displacements  $u_3(t)$  at point A for FEM solution can be attributed to the numerical damping.

We can observe from Figures 6, 7, 10, and 11 that BEM solutions for stresses exhibit relatively strong oscillations which occur due to the Gibbs phenomenon. The truncation of the frequency spectrum at  $\omega_{\max}$  causes oscillations in time-domain responses near jump discontinuities. A frequency-domain data windowing approach is used to alleviate the Gibbs oscillations. Before transferring frequency-domain response back into the time domain using Durbin's method, said response is multiplied at each frequency by some suitable data window function  $W(\omega_k)$ . And so, the magnitude of oscillations in time domain is reduced. Results of our extensive numerical testing of various window functions indicate that Hanning and Blackman windows often employed in frequency-domain BEM analysis yield overly smoothed results. We propose to use Riesz window:

$$W(\omega_k) = 1.0 - \left( \frac{\omega_k}{\omega_{\max}} \right)^2.$$

Figures 12 and 13 display the FEM results and post-processed with data windowing technique BEM solutions. Indeed, agreement between them improved significantly.



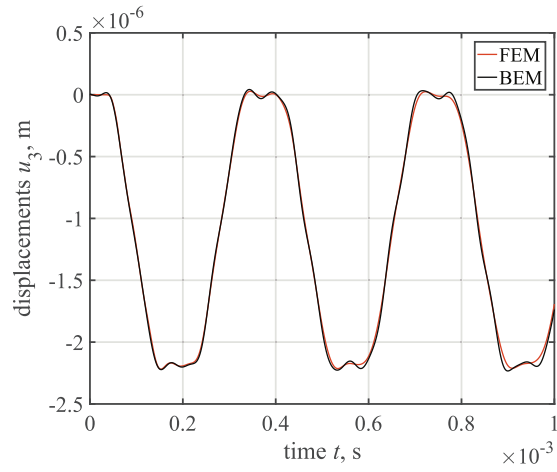


**Figure 9.** BEM and FEM solutions for displacements  $u_3(t)$  at point B.

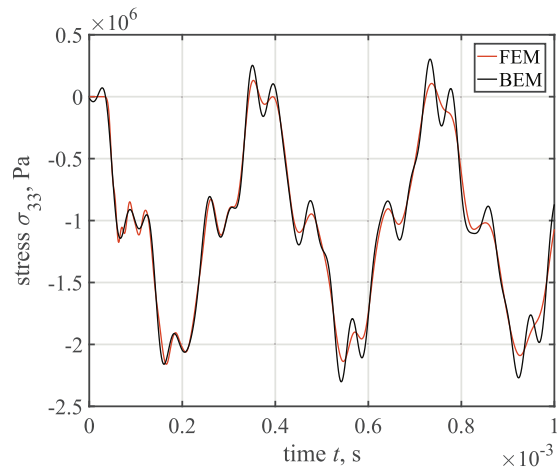


**Figure 10.** BEM and FEM solutions for stress  $\sigma_{33}(t)$  at point B.

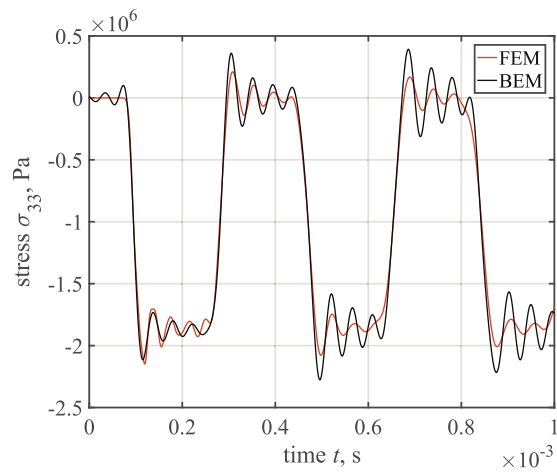


**Figure 11.** BEM and FEM solutions for stress  $\sigma_{33}(t)$  at point C.

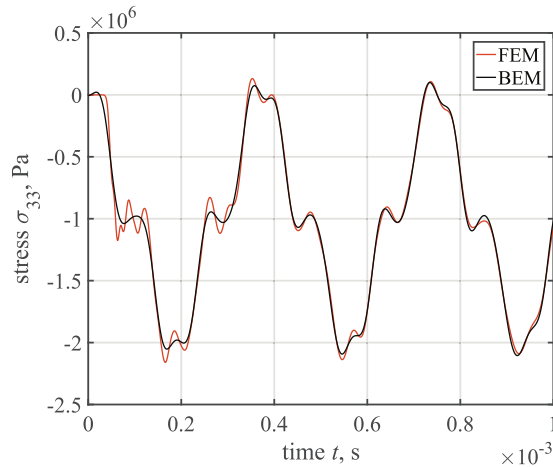


**Figure 12.** BEM solutions with data windowing for stress  $\sigma_{33}(t)$  at point B.

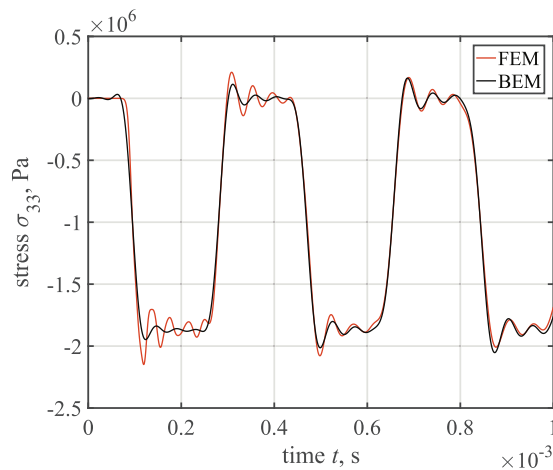


**Figure 13.** BEM solutions with data windowing for stress  $\sigma_{33}(t)$  at point C.

## 6. Conclusion

The obtained results allow us to conclude that the presented Laplace domain BEM coupled with the Durbin's method and frequency-domain data windowing technique is able to produce stable and accurate results for anisotropic elastodynamic analysis even for a low number of sampling frequencies. Moreover, in a further study, the presented framework can be readily applied to more complex structures and materials with coupled fields (piezoelectric, magnetoelastoelectric, etc). A lot of effort has been put to investigate different phenomena in such materials [40,41].





### Declaration of conflicting interests

The author(s) declared no potential conflicts of interest with respect to the research, authorship, and/or publication of this article.

### Funding

The author(s) disclosed receipt of the following financial support for the research, authorship, and/or publication of this article: Development of Laplace domain boundary element formulation was carried out with the financial support of the Ministry of Science and Higher Education of the Russian Federation (task 0729-2020-0054); development and numerical testing of frequency-domain data windowing technique were financially supported by the Russian Science Foundation under Grant No. 21-19-00283.

## ORCID iDs

Ivan Markov  <https://orcid.org/0000-0002-1776-2680>  
Leonid Igumnov  <https://orcid.org/0000-0003-3035-0119>  
Aleksandr Belov  <https://orcid.org/0000-0003-3704-048X>  
Victor Eremeyev  <https://orcid.org/0000-0002-8128-3262>

## References

- [1] Pak, RYS, and Guzina, BB. Seismic soil-structure interaction analysis by direct boundary element methods. *Int J Solids Struct* 1999; 36: 4743–4766.
- [2] Sáez, A, and Domínguez, J. BEM analysis of wave scattering in transversely isotropic solids. *Int J Num Method Eng* 1999; 44: 1283–1300.
- [3] Ahmad, S, Leyte, F, and Rajapakse, RKND. BEM analysis of two-dimensional elastodynamic problems of anisotropic solids. *J Eng Mech* 2001; 127: 149–156.
- [4] Niu, Y, and Dravinski, M. Direct 3D BEM for scattering of elastic waves in a homogeneous anisotropic half-space. *Wave Motion* 2003; 38: 165–175.
- [5] Niu, Y, and Dravinski, M. Three-dimensional BEM for scattering of elastic waves in general anisotropic media. *Int J Numer Meth Engng* 2003; 58: 979–998.
- [6] Chuhan, Z, Yuntao, R, Pekau, OA, et al. Time-domain boundary element method for underground structures in orthotropic media. *J Eng Mech* 2004; 130: 105–116.
- [7] Milazzo, A, Benedetti, I, and Aliabadi, MH. Hierarchical fast BEM for anisotropic time-harmonic 3-D elastodynamics. *Computers & Structures* 2012; 96–97: 9–24.
- [8] Barros, PLA. Impedances of rigid cylindrical foundations embedded in transversely isotropic soils. *Int J Numer Anal Meth Geomech* 2006; 30: 683–702.
- [9] Furukawa, A, Saitoh, T, and Hirose, S. Convolution quadrature time-domain boundary element method for 2-D and 3-D elastodynamic analyses in general anisotropic elastic solids. *Eng Anal Bound Element* 2014; 39: 64–74.
- [10] Ba, Z, and Gao, X. Soil-structure interaction in transversely isotropic layered media subjected to incident plane SH waves. *Shock Vibr* 2017; 2017: 1–13.
- [11] Pan, E, and Chen, W. *Static Green's functions in anisotropic media*. New York: Cambridge University Press, 2015.
- [12] Xie, L, Zhang, C, Sladek, J, et al. Unified analytical expressions of the three-dimensional fundamental solutions and their derivatives for linear elastic anisotropic materials. *Proc R Soc A* 2016; 472: 20150272.
- [13] Wang, C-Y, and Achenbach, JD. Elastodynamic fundamental solutions for anisotropic solids. *Geophys J Int* 1994; 118: 384–392.
- [14] Wang, C-Y, and Achenbach, JD. Three-dimensional time-harmonic elastodynamic Green's functions for anisotropic solids. *Proc R Soc Lond A* 1995; 449: 441–458.
- [15] Yildizdag, ME, Tran, CA, Barchiesi, E, et al. A multi-disciplinary approach for mechanical metamaterial synthesis: a hierarchical modular multiscale cellular structure paradigm. In: Altenbach, H, and Öchsner, A (eds) *State of the art and future trends in material modeling*. Cham: Springer, pp. 485–505.
- [16] Barchiesi, E, dell'Isola, F, Laudato, M, et al. A 1D continuum model for beams with pantographic microstructure: asymptotic micro-macro identification and numerical results. In: Dell'Isola, F, Eremeyev, VA, and Porubov, A (eds) *Advances in mechanics of microstructured media and structures*. Cham: Springer, pp. 43–74.
- [17] Dell'Isola, F, Turco, E, Misra, A, et al. Force–displacement relationship in micro-metric pantographs: experiments and numerical simulations. *Comptes Rend Mécan* 2019; 347: 397–405.
- [18] Barchiesi, E, Eugster, SR, dell'Isola, F, et al. Large in-plane elastic deformations of bi-pantographic fabrics: asymptotic homogenization and experimental validation. *Math Mech Solids* 2020; 25: 739–767.
- [19] Yildizdag, ME, Barchiesi, E, and dell'Isola, F. Three-point bending test of pantographic blocks: numerical and experimental investigation. *Math Mech Solids* 2020; 25: 1965–1978.
- [20] Dell'Isola, F, Corte, AD, and Giorgio, I. Higher-gradient continua: the legacy of Piola, Mindlin, Sedov and Toupin and some future research perspectives. *Math Mech Solids* 2017; 22: 852–872.
- [21] Dell'Isola, F, Della Corte, A, Greco, L, et al. Plane bias extension test for a continuum with two inextensible families of fibers: a variational treatment with Lagrange multipliers and a perturbation solution. *Int J Solids Struct* 2016; 81: 1–12.
- [22] Dell'Isola, F, Giorgio, I, Pawlikowski, M, et al. Large deformations of planar extensible beams and pantographic lattices: heuristic homogenization, experimental and numerical examples of equilibrium. *Proc R Soc A* 2016; 472: 20150790.
- [23] Placidi, L, Andreaus, U, and Giorgio, I. Identification of two-dimensional pantographic structure via a linear D4 orthotropic second gradient elastic model. *J Eng Math* 2017; 103: 1–21.
- [24] Spagnuolo, M, Franciosi, P, and dell'Isola, F. A Green operator-based elastic modeling for two-phase pantographic-inspired bi-continuous materials. *Int J Solids Struct* 2020; 188–189: 282–308.



- [25] Boutin, C, and dell'Isola, F. Green's functions and integral representation of generalized continua: the case of orthogonal pantographic lattices. *Z Angew Math Phys* 2021; 72: 58.
- [26] Durbin, F. Numerical inversion of Laplace transforms: an efficient improvement to Dubner and Abate's method. *Comput J* 1974; 17: 371–376.
- [27] Zhao, X. An efficient approach for the numerical inversion of Laplace transform and its application in dynamic fracture analysis of a piezoelectric laminate. *Int J Solids Struct* 2004; 41: 3653–3674.
- [28] Kuhlman, KL. Review of inverse Laplace transform algorithms for Laplace-space numerical approaches. *Numer Algor* 2013; 63: 339–355.
- [29] Ing, Y-S, Liao, H-F, and Huang, K-S. The extended Durbin method and its application for piezoelectric wave propagation problems. *Int J Solids Struct* 2013; 50: 4000–4009.
- [30] Xiao, J, Ye, W, and Wen, L. Efficiency improvement of the frequency-domain BEM for rapid transient elastodynamic analysis. *Comput Mech* 2013; 52: 903–912.
- [31] Raoofian Naeeni, M, Campagna, R, Eskandari-Ghadi, M, et al. Performance comparison of numerical inversion methods for Laplace and Hankel integral transforms in engineering problems. *Appl Math Comput* 2015; 250: 759–775.
- [32] Schanz, M, Ye, W, and Xiao, J. Comparison of the convolution quadrature method and enhanced inverse FFT with application in elastodynamic boundary element method. *Comput Mech* 2016; 57: 523–536.
- [33] Adamek, V, Vales, F, and Cerv, J. Numerical Laplace inversion in problems of elastodynamics: comparison of four algorithms. *Adv Eng Softw* 2017; 113: 120–129.
- [34] Crump, KS. Numerical inversion of Laplace transforms using a Fourier series approximation. *J ACM* 1976; 23: 89–96.
- [35] Wang, C-Y, and Denda, M. 3D BEM for general anisotropic elasticity. *Int J Solids Struct* 2007; 44: 7073–7091.
- [36] Benedetti, I, Milazzo, A, and Aliabadi, MH. Fast hierarchical boundary element method for large-scale 3-D elastic problems. In: Aliabadi, MH, and Wen, PH (eds) *Boundary element methods in engineering and sciences*. London: Imperial College Press, pp. 145–195.
- [37] Fedorov, FI. *Theory of elastic waves in crystals*. Boston, MA: Springer, 1968.
- [38] Gaul, L, Kögl, M, and Wagner, M. *Boundary element methods for engineers and scientists*. Berlin, Heidelberg: Springer, 2003.
- [39] Clough, RW, and Penzien, J. *Dynamics of structures*. Berkeley, CA: Computers and Structures, 2003.
- [40] Abali, BE, and Reich, FA. Thermodynamically consistent derivation and computation of electro-thermo-mechanical systems for solid bodies. *Comput Method Appl Mech Eng* 2017; 319: 567–595.
- [41] Abali, BE, and Queiruga, AF. Theory and computation of electromagnetic fields and thermomechanical structure interaction for systems undergoing large deformations. *J Comput Phys* 2019; 394: 200–231.

